POTSDAM-INSTITUT FÜR KLIMAFOLGENFORSCHUNG

Chaos
An Interdisciplinary Journal of Nonlinear Science

RESEARCH ARTICLE | AUGUST 14 2023

Bursting multistability induced by double-Hopf bifurcation

Special Collection: Regime switching in coupled nonlinear systems: sources, prediction, and control

Yibo Xia ; Serhiy Yanchuk ; Yichuan Cao ; Qinsheng Bi ; Jürgen Kurths

Chaos 33, 083137 (2023)
https://doi.org/10.1063/5.0157718

Bursting multistability induced by double-Hopf bifurcation

Cite as: Chaos 33, 083137 (2023); doi: 10.1063/5.0157718
Submitted: 10 May 2023 · Accepted: 7 July 2023 ·
Published Online: 14 August 2023

Yibo Xia,[1,2] Serhiy Yanchuk,[2,3] Yichuan Cao,[4] Qinsheng Bi,[1,a)] and Jürgen Kurths[2,5]

AFFILIATIONS

[1]Faculty of Civil Engineering and Mechanics, Jiangsu University, Zhenjiang 212013, People's Republic of China
[2]Potsdam Institute for Climate Impact Research (PIK), Potsdam 14473, Germany
[3]Department of Mathematics, Humboldt University Berlin, Berlin 12489, Germany
[4]Department of Mechanical Engineering, University of South Carolina, Columbia, South Carolina 29208, USA
[5]Department of Physics, Humboldt University Berlin, Berlin 12489, Germany

Note: This paper is part of the Focus Issue on Regime switching in coupled nonlinear systems: sources, prediction, and control.
[a)]**Author to whom correspondence should be addressed:** qbi@ujs.edu.cn

ABSTRACT

We study the slow–fast dynamics of a system with a double-Hopf bifurcation and a slowly varying parameter. The model consists of coupled Bonhöffer–van der Pol oscillators excited by a periodic slow-varying AC source. We consider two cases where the slowly varying parameter passes by or crosses the double-Hopf bifurcation, respectively. Due to the system's multistability, two bursting solutions are observed in each case: single-mode bursting and two-mode bursting. Further investigation reveals that the double-Hopf bifurcation causes a stable coexistence of these two bursting solutions. The mechanism of such coexistence is explained using the slowly changing phase portraits of the fast subsystem. We also show the robustness of the observed effect in the vicinity of the double-Hopf bifurcation.

Bursting oscillations have been widely reported in natural and technological systems. The alternation between large-amplitude oscillations (spiking states) and small-amplitude oscillations or at rest (quiescent states) in such systems is explained by different transitions through bifurcations. Here, we have discovered an effect of the codimension-2 double-Hopf bifurcation: it leads to the coexistence of different bursting solutions. Our projection technique based on singular value decomposition helps us to understand the multiple paths to bursting in the vicinity of the double-Hopf bifurcation.

I. INTRODUCTION

Many real-world problems involve multiple time scale dynamics.[1–7] For example, slow–fast chemical reaction systems with strongly different reaction rates can exhibit mixed-mode oscillations (MMOs),[8–11] corresponding to interactions of multiple periodic orbits; mixed-mode oscillations in a three-time-scale neural model are reported in Ref. 12 and the enhancement or emergence of bursting by noise in Refs. 13–17, to name but a few.

To understand the mechanism of bursting activities, Rinzel used the slow–fast analysis method,[18] based on splitting of the original system into fast and slow subsystems

$$\begin{aligned} \dot{x} &= f(x, y, \mu), \\ \dot{y} &= \varepsilon g(x, y, \mu), \end{aligned} \tag{1}$$

which can be treated separately under certain conditions. In particular, $0 < \varepsilon \ll 1$ implies that the fast variables x evolve at a much higher rate than the slow variables y. By treating y as a slowly varying parameter, equilibrium branches and bifurcations of the fast subsystem can be studied to explore the dynamics of transitions between spiking and quiescent states, and thus to classify different patterns of bursting oscillations. Based on this method, several results related to codimension-1 bifurcations of the fast subsystem have been obtained. For example, the fold/fold, fold/Hopf, and fold/homoclinic bursting attractors have been reported in Refs. 19 and 20. Izhikevich proposed a classification of possible bursting attractors in low-dimensional systems, refining the classification of codimension-1 bursts.[21]

However, higher codimension (higher than 1) bifurcations of the fast subsystem can lead to more complex forms of transitions.[22,23]

One such example is a bursting attractor with cusp bifurcation.[24] By changing the slowly varying parameter, not only interactions between stable attractors can be observed but also different bifurcation paths.[25] A question that arises is how a high codimension bifurcation can affect transitions in slow–fast systems,[26] or, more generally, whether there are differences between bursting oscillations due to codimension-1 or codimension-2 bifurcations of the fast subsystem.

So far, a limited number of studies have been devoted to the slow–fast dynamics of systems with high codimension bifurcations of the fast subsystem.[26–31] The papers[27,32] investigated how bursting dynamics arise when the slow parameter periodically follows a closed path around the codimension-2 cusp, degenerate Hopf, Bogdanov–Takens, zero-Hopf, and double-Hopf bifurcation points. The bursting attractors in the Chay system related to codimension-2 cusp and Bogdanov–Takens bifurcations were reported in Refs. 26 and 28, which show that codimension-2 bifurcations can determine the bursting types. The paper[29] provides complex bursting patterns associated with a codimension-2 global bifurcation involving a saddle-node bifurcation of equilibrium and a saddle-node bifurcation of the limit cycle. The burst duration and the interburst interval are shown to be controlled by such a global bifurcation. Furthermore, the slow–fast dynamics in the presence of codimension-2 pitchfork-Hopf bifurcation was studied in our recent work.[31]

Among the codimension-2 bifurcations discussed, the double-Hopf bifurcation is characterized by the occurrence of two pairs of purely imaginary roots, giving rise to two periodic solutions. With the variation of parameters, such a phenomenon can result in various possible transitions, e.g., from a stable state to oscillatory behavior, from one oscillatory behavior to another, even route to chaos via a homoclinic bifurcation in the vicinity of the bifurcation point.[33] Understanding the slow–fast dynamics with the double-Hopf bifurcation remains an open problem.

Here, we study two coupled Bonhöffer–van der Pol (BVP) oscillators.[34] This five-dimensional system can exhibit codimension-2 double-Hopf bifurcation leading to the birth of two stable limit cycles.[35] The system also features multistability so that various transitions can be observed near the double-Hopf bifurcation. Additionally, we consider a periodically changing power source as a slowly varying excitation to the circuit. This type of external force can potentially be implemented in hardware.

Our work focuses on the bursting multistability induced by the double-Hopf bifurcation. More specifically, we observe two bursting solutions: single-mode bursting and two-mode bursting. The single-mode bursting contains fast oscillations based on a single limit cycle, while the two-mode bursting involves fast oscillations from two different limit cycles. Near the double-Hopf point, the two different bursting scenarios coexist, i.e., depending on the amplitude of the variation of the slow parameter, either single-mode or two-mode bursting can be realized. The mechanism for such coexistence is explained using phase space analysis of the fast subsystem. We also show the robustness of the observed effect.

The structure of the paper is as follows. In Sec. II, we introduce the mathematical model and its dynamical properties. In particular, we consider two-parameter paths that allow the slowly varying parameter to pass by (codimension 1 case) and cross (codimension 2 case) the double-Hopf bifurcation point. In Secs. III and IV, we present two solutions of bursting and the bursting multistability. We investigate the fast subsystem phase portraits in Sec. V to explain the mechanism of transitions between two limit cycles. We also explore the robustness of the double-Hopf effect on bursting multistability.

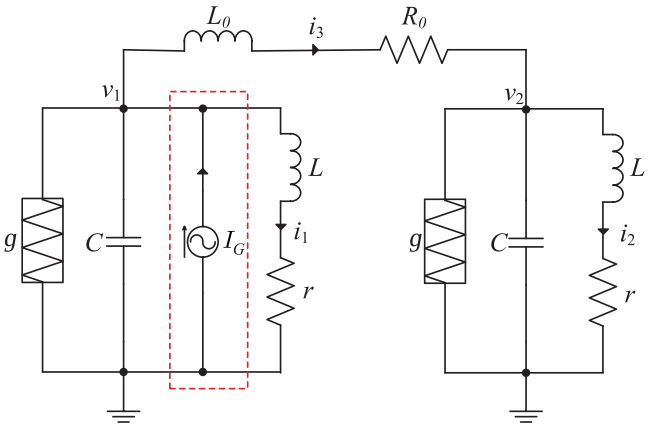

FIG. 1. The circuit diagram. Two Bonhöffer–van der Pol (BVP) oscillators are coupled by a resistor–inductor component L_0 and R_0. L, r, and C represent the inductor, resistor, and capacitor in two oscillators, respectively. g is a nonlinear conductor.[36,37]

II. MODEL AND ITS DYNAMICAL PROPERTIES

The considered system is constructed by connecting two identical BVP oscillators with a resistor–inductor component[34] shown in Fig. 1. We introduce a periodically changing current source to the circuit $I_G = i_G \sin(\varepsilon t)$. The dynamics of the circuit is described by the following five-dimensional system of equations:

$$\begin{aligned} L\frac{di_1}{dt} &= v_1 - ri_1, \\ C\frac{dv_1}{dt} &= -i_1 - g(v_1) - i_3 + i_G \sin(\varepsilon t), \\ L\frac{di_2}{dt} &= v_2 - ri_2, \\ C\frac{dv_2}{dt} &= -i_2 - g(v_2) + i_3, \\ L_0\frac{di_3}{dt} &= v_1 - v_2 - R_0 i_3, \end{aligned} \tag{2}$$

where L, L_0, C, and R_0 are positive parameters and $i_{1,2,3}$ and $v_{1,2}$ represent the currents and voltages, respectively. The relationship between currents and voltages through nonlinear conductance is given by the function $g(v) = d_1 v + d_3 v^3 + d_5 v^5$.

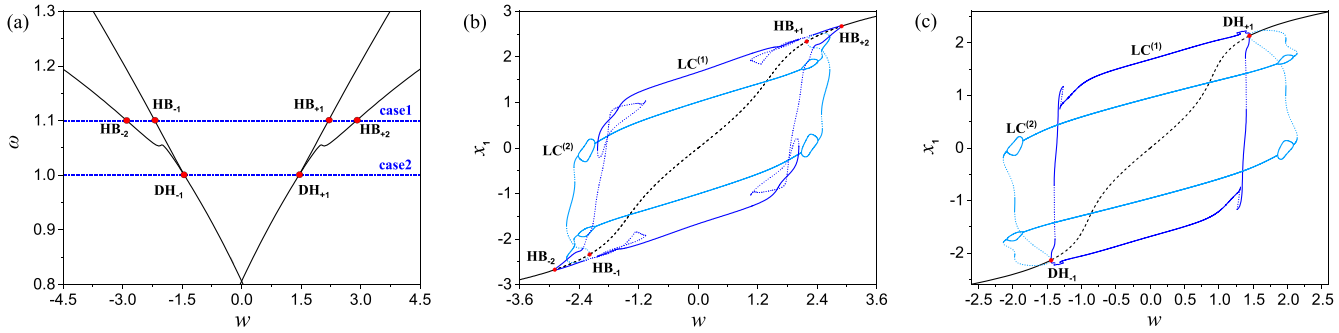

FIG. 2. Bifurcation diagrams for system (3). (a) Hopf bifurcations of the equilibrium in the (w, ω) plane. (b) One-parameter bifurcation diagram for $\omega = 1.1$ and varying w. (c) One-parameter bifurcation diagram for $\omega = 1.0$ and varying w. The black curves in (b) and (c) refer to the equilibrium points and the blue and light blue curves represent two different limit cycles. $DH_{\pm1}$: double-Hopf bifurcations; $HB_{\pm1}$ and $HB_{\pm2}$: Hopf bifurcations for $\omega = 1.1$; $LC^{(1)}$ and $LC^{(1)}$: branches of limit cycles. Other parameters are $\sigma = 0.5, \alpha = -1.0, \beta = -1.0, \gamma = 0.7, \omega_0 = 1.0, \sigma_0 = 0.2011$. Details of bifurcation diagrams are shown in Appendixes B and C.

Similar to Ref. 34, we rescale system (2) as follows:

$$\begin{aligned}
\dot{x}_1 &= \omega y_1 - \sigma x_1, \\
\dot{y}_1 &= -\alpha y_1 - \beta y_1^3 - \gamma y_1^5 - \omega x_1 - \omega_0 x_3 + w, \\
\dot{x}_2 &= \omega y_2 - \sigma x_2, \\
\dot{y}_2 &= -\alpha y_2 - \beta y_2^3 - \gamma y_2^5 - \omega x_2 + \omega_0 x_3, \\
\dot{x}_3 &= -\sigma_0 x_3 + \omega_0 (y_1 - y_2),
\end{aligned} \tag{3}$$

where $w = A\sin(\varepsilon t)$, $A = \frac{i_G}{\sqrt{C}}$, $x_{1,2} = \sqrt{L}\, i_{1,2}$, $y_{1,2} = \sqrt{C}\, v_{1,2}$, $x_3 = \sqrt{L_0}\, i_3$, $\omega = \frac{1}{\sqrt{LC}}$, $\omega_0 = \frac{1}{\sqrt{L_0 C}}$, $\sigma = \frac{r}{L}$, $\sigma_0 = \frac{R_0}{L_0}$, $\alpha = \frac{d_1}{C}$, $\beta = \frac{d_3}{C^2}$, and $\gamma = \frac{d_5}{C^3}$.

For the non-excited system ($i_G = 0$), a double-Hopf bifurcation and two coexisting periodic orbits have been reported for a particular set of parameters.[35] Furthermore, single-scroll and double-scroll chaotic attractors have been shown in Ref. 36. In addition, other bifurcations of the equilibrium point and limit cycle can occur in the

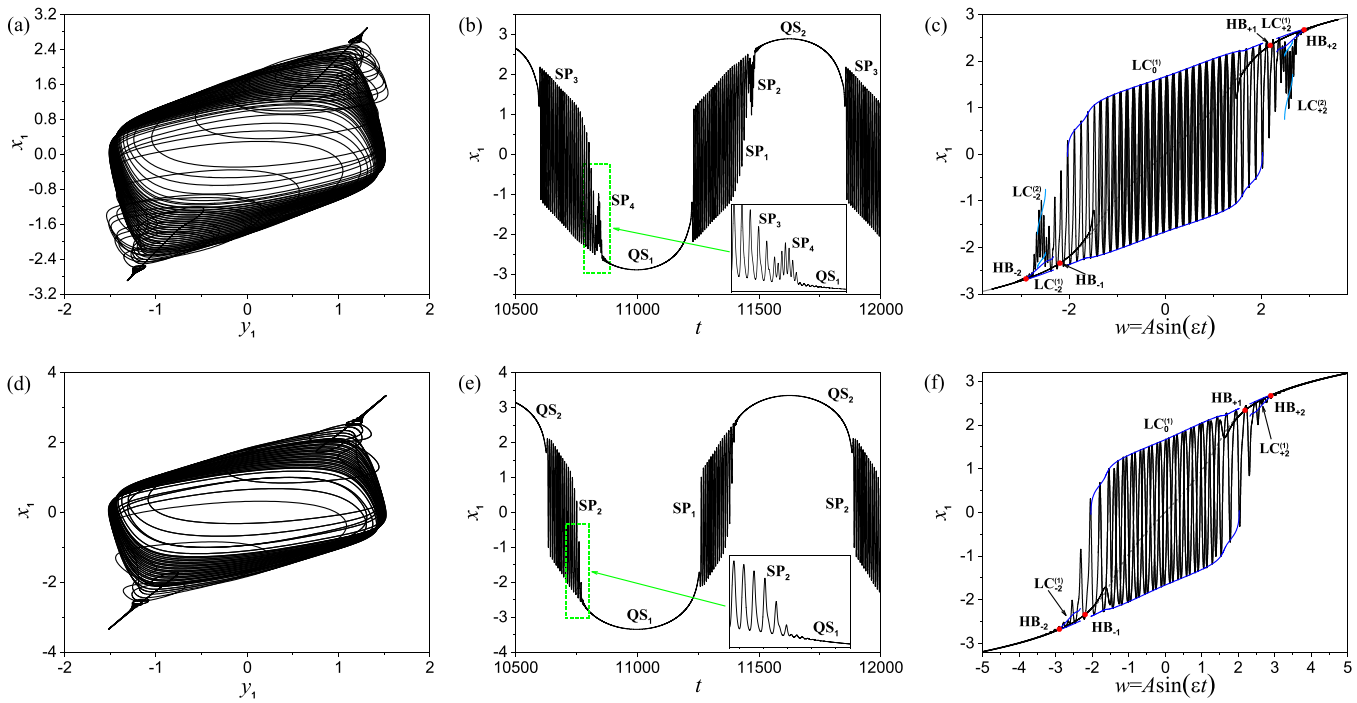

FIG. 3. Two bursting solutions in the codimension-1 case. (a)–(c) The two-mode bursting attractor, timeseries, and the overlap of the phase portrait, and the bifurcation diagram for $A = 3.60$. (d)–(f) The single-mode bursting attractor, timeseries, and the overlap of the phase portrait and the bifurcation diagram for $A = 6.0$. Other parameters are $\omega = 1.1, \sigma = 0.5, \alpha = -1.0, \beta = -1.0, \gamma = 0.7, \omega_0 = 1.0, \sigma_0 = 0.2011, \varepsilon = 0.005$.

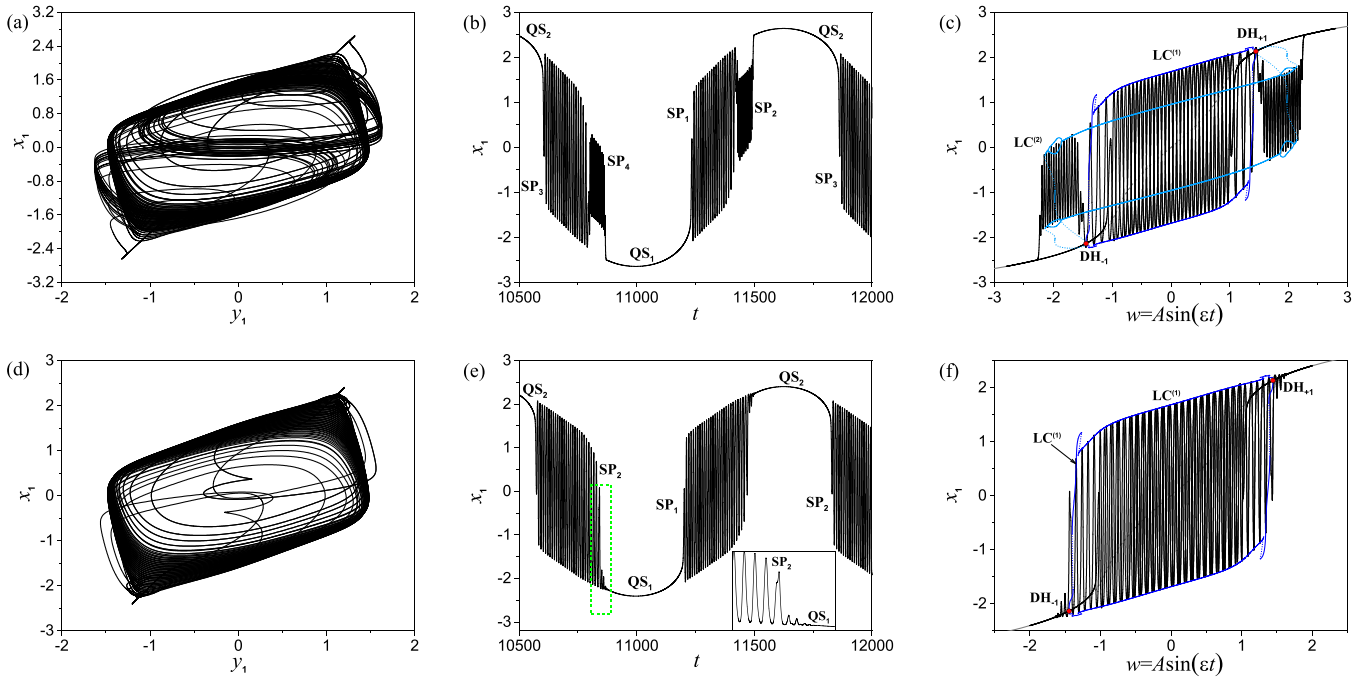

FIG. 4. Two bursting solutions in codimension-2 case. (a)–(c) The two-mode bursting attractor, timeseries, and the overlap of the phase portrait and the bifurcation diagram for $A = 2.80$. (d)–(f) The single-mode bursting attractor, timeseries, and the overlap of the phase portrait and the bifurcation diagram for $A = 2.0$. Other parameters are: $\omega = 1.1, \sigma = 0.5, \alpha = -1.0, \beta = -1.0, \gamma = 0.7, \omega_0 = 1.0, \sigma_0 = 0.2011, \varepsilon = 0.005$.

neighborhood of the double-Hopf bifurcation, such as homoclinic and Neimark–Sacker bifurcations,[33] leading to complex dynamics.

For the excited system (3), we first consider the excitation term w as the control parameter and the other parameters fixed at $\sigma = 0.5, \alpha = -1.0, \beta = -1.0, \gamma = 0.7, \omega_0 = 1.0$, and $\sigma_0 = 0.2011$. The two-parameter bifurcation diagram in the (w, ω) plane in Fig. 2(a) shows the Hopf bifurcations of the equilibrium. We see that two pairs of symmetric Hopf bifurcations divide the parameter plane into five regions. The Hopf lines are tangent at point $DH_{\pm 1}$ with $w = 1.4437, \omega = 1.000$, implying a pair of double-Hopf bifurcations. The corresponding eigenvalues are $\lambda_1 = -0.4057$, $\lambda_{2,3} = \pm 1.5739i$, and $\lambda_{4,5} = \pm 0.9552i$.

To study the effect of the double-Hopf bifurcation, we analyze the case $\omega = 1.0$, for which the double-Hopf occurs, and $\omega = 1.1$, for which only codimension-1 bifurcations take place. Figures 2(b) and 2(c) show the one-parameter bifurcation diagrams for the branches of equilibria and limit cycles. Details of the dynamical behaviors in each case are given in Appendixes A–D. The two bifurcation diagrams have certain similarities: The equilibrium branches lose stability via a pair of symmetric Hopf (double-Hopf) bifurcations. The limit cycles branch $LC^{(2)}$ of relatively small amplitude undergoes period-doubling and fold bifurcations and then disappears at Hopf (double-Hopf) bifurcations. The limit cycle branch $LC^{(1)}$ of larger amplitude coexists with $LC^{(1)}$ for a certain interval and loses its stability via fold bifurcations of limit cycles.

The main difference between the scenarios of Figs. 2(b) and 2(c) is that the two branches of the limit cycles emerge from the double-Hopf bifurcation in Fig. 2(c), whereas each branch emerges from the single Hopf bifurcation in Fig. 2(b). There is also a coexistence of stable equilibria and limit cycles in Fig. 2(c). In the following, we will show how the above mentioned features lead to substantially different properties of the bursting solutions in the system with slow periodic excitation.

III. SINGLE-MODE AND TWO-MODE BURSTING

We fix the excitation frequency at $\varepsilon = 0.005$ in system (3) so that the parameter w becomes a non-autonomous slowly varying term that crosses the two Hopf bifurcations or the double-Hopf bifurcation, respectively. As a result of such a crossing, bursting solutions appear in both cases: $\omega = 1.0$ and $\omega = 1.1$.

We first illustrate the two bursting solutions in the codimension-1 case for $\omega = 1.1$. Figure 3 shows the phase portraits and corresponding timeseries of two types of bursting attractors: Figs. 3(a)–3(c) for two-mode bursting, and Figs. 3(d)–3(f) for single-mode bursting. The main difference is that the two-mode bursts contain two parts, each with a different amplitude and frequency. We identify the connected parts of the bursts with similar amplitude and frequency as "spiking states." One can see from the timeseries that the two-mode bursting attractor has four spiking states and two quiescent states, namely, $SP_i, i = 1, 2, 3, 4$ and $QS_i, i = 1, 2$, whereas the single-mode bursting attractor has two spiking states SP_i, $i = 1, 2$. The frequency of spiking states $SP_{2,4}$ in two-mode bursts

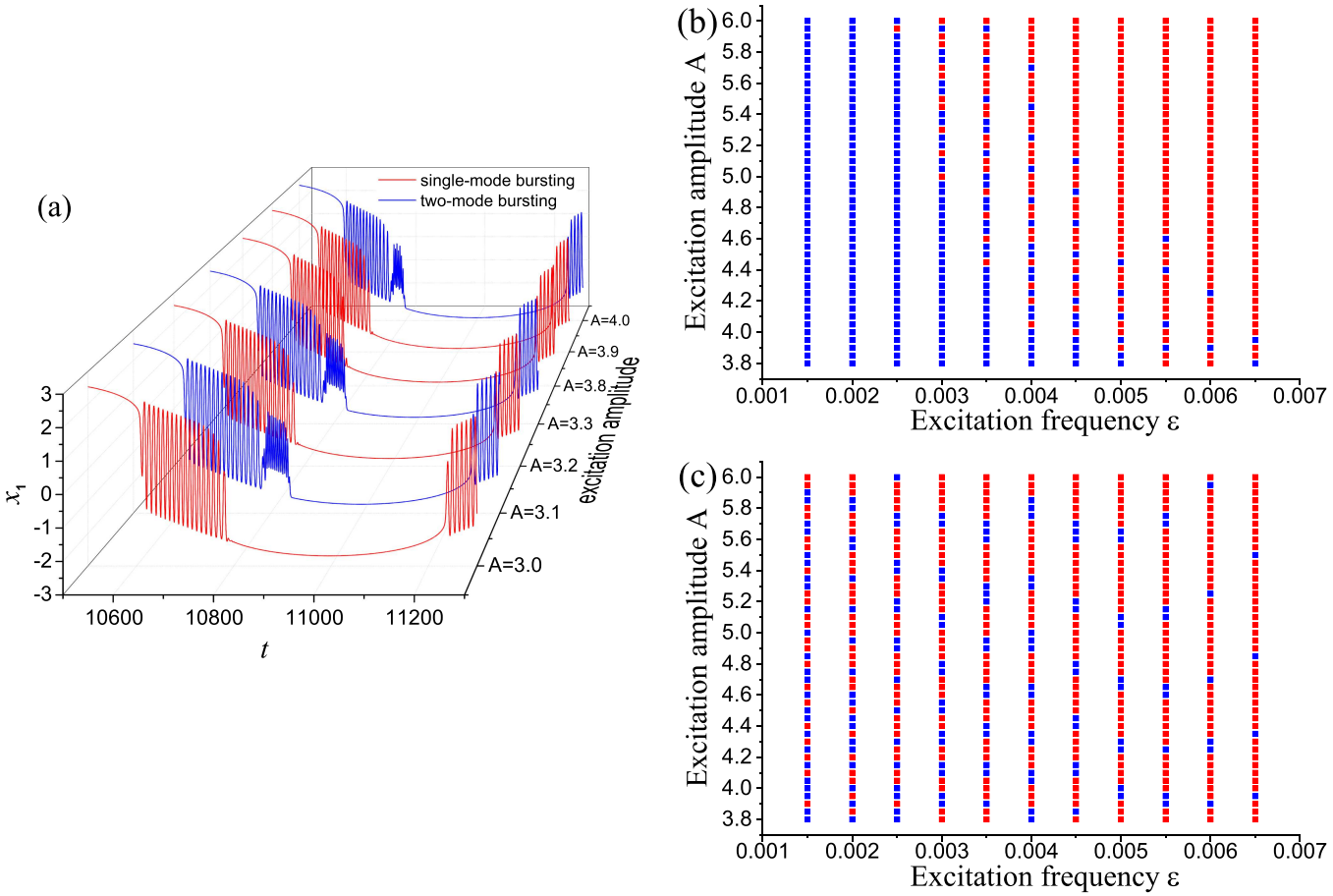

FIG. 5. The bursting multistability. (a) Bursting solutions for different excitation amplitude A. One can observe single-mode (red trajectories) and two-mode bursting (blue trajectories). (b) Distribution of two bursting solutions in the (A, ε) plane in the codimension-1 case. (c) Distribution of two bursting solutions in the (A, ε) plane in the codimension-2 case. Red points represent the single-mode bursting while blue the two-mode bursting.

is larger than the frequency in $SP_{1,3}$, suggesting the transitions from one limit cycle of the fast subsystem to another.

To further clarify the transitions, we show the overlap of the phase portrait and the bifurcation diagram in Fig. 3 (right column). In the two-mode bursting regime, the trajectory moving along the large-amplitude oscillations $LC^{(1)}$ is then attracted by the smaller-amplitude oscillations in $LC^{(2)}$, which is bifurcated from super-critical Hopf bifurcations $HB_{\pm 2}$ and $HB_{\pm 1}$, respectively. In contrast, the trajectory of the single-mode bursting settles to the equilibrium after moving along $LC^{(1)}$.

Similarly, two types of bursting solutions are present in the codimension-2 case as shown in Fig. 4. A more pronounced transition between the spiking states SP_1 and SP_2 is observed, suggesting that different transition mechanisms may be involved compared to the codimension-1 case. Figure 4 (right column), combining the bifurcation diagram and the trajectories, further clarifies that the two solutions of bursting oscillations in the double-Hopf case are related to the bistability of the equilibrium and the limit cycle $LC^{(2)}$ from double-Hopf bifurcation point $DH_{\pm 1}$.

From the two solutions of bursting in the codimension-1 and codimension-2 cases, we can conclude that the appearance of single-mode and two-mode bursting is due to the coexistence of stable attractors in the fast subsystem, while the bifurcation mechanisms of this coexistence are different. In Sec. IV, we will discuss the emergence and the coexistence of the two different bursting regimes in more detail.

IV. BURSTING MULTISTABILITY

In this section, we consider the effects of the excitation amplitude A and the frequency ε on the emergence of bursting oscillations in system (3). Note that variations in ε can affect the transition delay between different states in a slow–fast system and, thus, determine to which attractor of the fast subsystem the trajectory will converge.[38]

Figure 5(a) shows the bursting timeseries for the same excitation frequency $\varepsilon = 0.005$ but different excitation amplitudes A in the codimension-2 case. Two solutions of bursting appear for

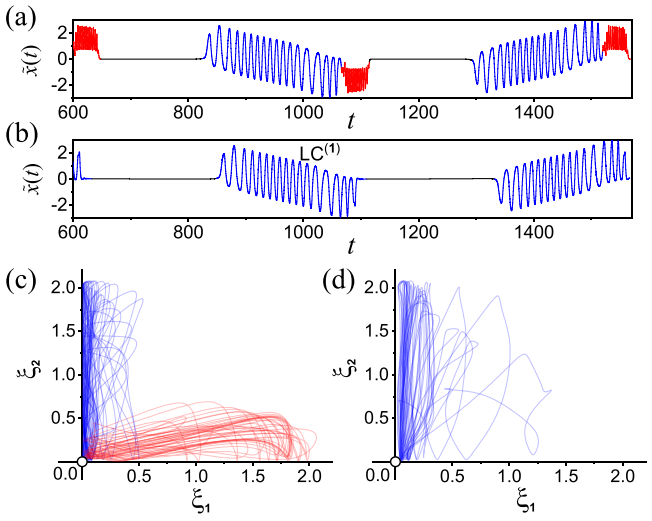

FIG. 6. The bursting solutions and their projections on subspaces. (a) The solution $\tilde{x}(t)$ of the two-mode bursting for $A = 3.0$. (b) The solution $\tilde{x}(t)$ of the single-mode bursting for $A = 3.2$. (c) and (d) The projections of two bursting solutions on subspaces defined by (6). Blue lines represent oscillations according to $LC^{(1)}$, and red lines represent oscillations according to $LC^{(2)}$. Other parameters are $\sigma = 0.5, \alpha = -1.0, \beta = -1.0, \gamma = 0.7, \omega_0 = 1.0, \sigma_0 = 0.2011, \omega = 1.0, \varepsilon = 0.005$.

different values of the excitation amplitude, e.g., the two-mode bursting appears for $A = 3.1$, $A = 3.3$, and $A = 4.0$.

Importantly, the distribution of the single- and two-mode bursting is different for the codimension-1 and codimension-2 cases [cf. Figs. 5(b) and 5(c)]. The blue squares denote the two-mode bursting, and the red dots represent the single-mode bursting that are observed for different values of A and ε. In the codimension-1 case, two-mode bursting is always found for a sufficiently small excitation frequency $\varepsilon < 0.02$. As the excitation frequency increases, the single-mode bursting is predominantly observed. The distribution in the codimension-1 case shows that the appearance of single-mode and two-mode bursting depends strongly on the rate of change ε, suggesting that different slow passage effects influence the choice of the attractor for the fast subsystem, similar to the rate-induced tipping.[39] In the codimension-2 case, we still observe the influence of slow passage effects at relatively high excitation frequencies—there are fewer blue squares in the distribution. However, the two solutions of bursting always appear with the variation of the excitation amplitude A, for all excitation frequencies. This interesting observation implies that the single-mode bursting coexists with the two-mode bursting for the double-Hopf case, at least for the range of the considered values of ε. We call this phenomenon as *bursting multistability* and will study it in more detail below.

V. SLOW–FAST ANALYSIS OF TRANSITIONS BETWEEN ATTRACTORS OF THE FAST SUBSYSTEM

This section investigates transitions between attractors of the fast subsystem with a slow change of w. We will also explain, why the single- and two-mode bursting coexist in the case of double-Hopf for arbitrary slow change rate ε.

As one can see from the bifurcation diagrams in Fig. 2, the phase portraits of the five-dimensional system (3) contain one, two, or three stable coexisting attractors depending on the value of the parameter w. One of them is the equilibrium, and the other two are limit cycles. In the following, we construct such a coordinate transformation that maps each stable attractor into a point in a two-dimensional plane (ξ_1, ξ_2). Here, ξ_1 and ξ_2 are two new coordinates playing the role analogous to the normal form coordinates in the case of double-Hopf bifurcation,[33] i.e., $(\xi_1, \xi_2) = (0, 0)$ corresponds to the equilibrium and $(\xi_1^*, 0)$ and $(0, \xi_2^*)$ to the two limit cycles with nonzero $\xi_{1,2}^*$. To construct the coordinates (ξ_1, ξ_2), we do not use the normal form theory, but the singular value decomposition and appropriate projections. As a result, the numbers ξ_1 and ξ_2 can be computed not only in a neighborhood of the double-Hopf point but also globally.

For a trajectory segment of the bursting oscillations, denoted by

$$x(t, t + \Delta t) = \{x(\tau),\ \tau \in (t, t + \Delta t)\},$$

the corresponding time series of the slowly varying parameter is $w(t, t + \Delta t)$. We also denote by $\phi_w^{(1)}(t)$ and $\phi_w^{(2)}(t)$, the limit cycles from the branches $LC^{(1)}$ and $LC^{(2)}$, respectively. $x_E(w)$ is the coordinate of the equilibrium point computed in Appendix A.

First, we shift the coordinates so that the equilibrium point is moved to the origin

$$\begin{aligned} \tilde{x}(t) &= x(t) - x_E(w(t)), \\ \tilde{\phi}_w^{(1)}(t) &= \phi_w^{(1)}(t) - x_E(w), \\ \tilde{\phi}_w^{(2)}(t) &= \phi_w^{(2)}(t) - x_E(w). \end{aligned} \tag{4}$$

For the next step, we introduce the three-dimensional subspaces $V_w^{(1)}$ and $V_w^{(2)}$, corresponding to the two limit cycles $\phi_w^{(1)}(t)$ and $\phi_w^{(2)}(t)$. The construction is based on the singular value decomposition (SVD). For any w, these subspaces can be defined as

$$\begin{aligned} V_w^{(1)} &= \langle v_1(w), v_2(w), v_3(w) \rangle, \\ V_w^{(2)} &= \langle v_1'(w), v_2'(w), v_3'(w) \rangle, \end{aligned} \tag{5}$$

where the $v_{1,2,3}(w)$ and $v'_{1,2,3}(w)$ are mutually orthogonal leading left singular vectors from SVD of $\phi_w^{(1)}(t)$ and $\phi_w^{(2)}(t)$, respectively. More precisely, let

$$M_w^{(1)} = \left[\phi_w^{(1)}(0), \phi_w^{(1)}(h_1), \phi_w^{(1)}(2h_1), \ldots, \phi_w^{(1)}(T_w^{(1)})\right]$$

and

$$M_w^{(2)} = \left[\phi_w^{(2)}(0), \phi_w^{(2)}(h_2), \phi_w^{(2)}(2h_2), \ldots, \phi_w^{(2)}(T_w^{(2)})\right]$$

be the $5 \times N$-dimensional matrices containing the discretized periodic solutions $\phi_w^{(1)}(t)$ and $\phi_w^{(2)}(t)$, with the stepsizes $h_i = T_w^{(i)}/N$, periods $T_w^{(i)}$, and N is the number of the discretization points. The stable and unstable limit cycles at each $w(t)$ as well as their periods are obtained from the parameter continuation using MATCONT.[40] Furthermore, periodic solutions from the family of stable limit cycle can be obtained by a direct computation of the fast subsystem.

The matrices $M_w^{(1)}$ and $M_w^{(2)}$ contain the elements we need to describe V_w^1 and V_w^2. The corresponding SVD gives

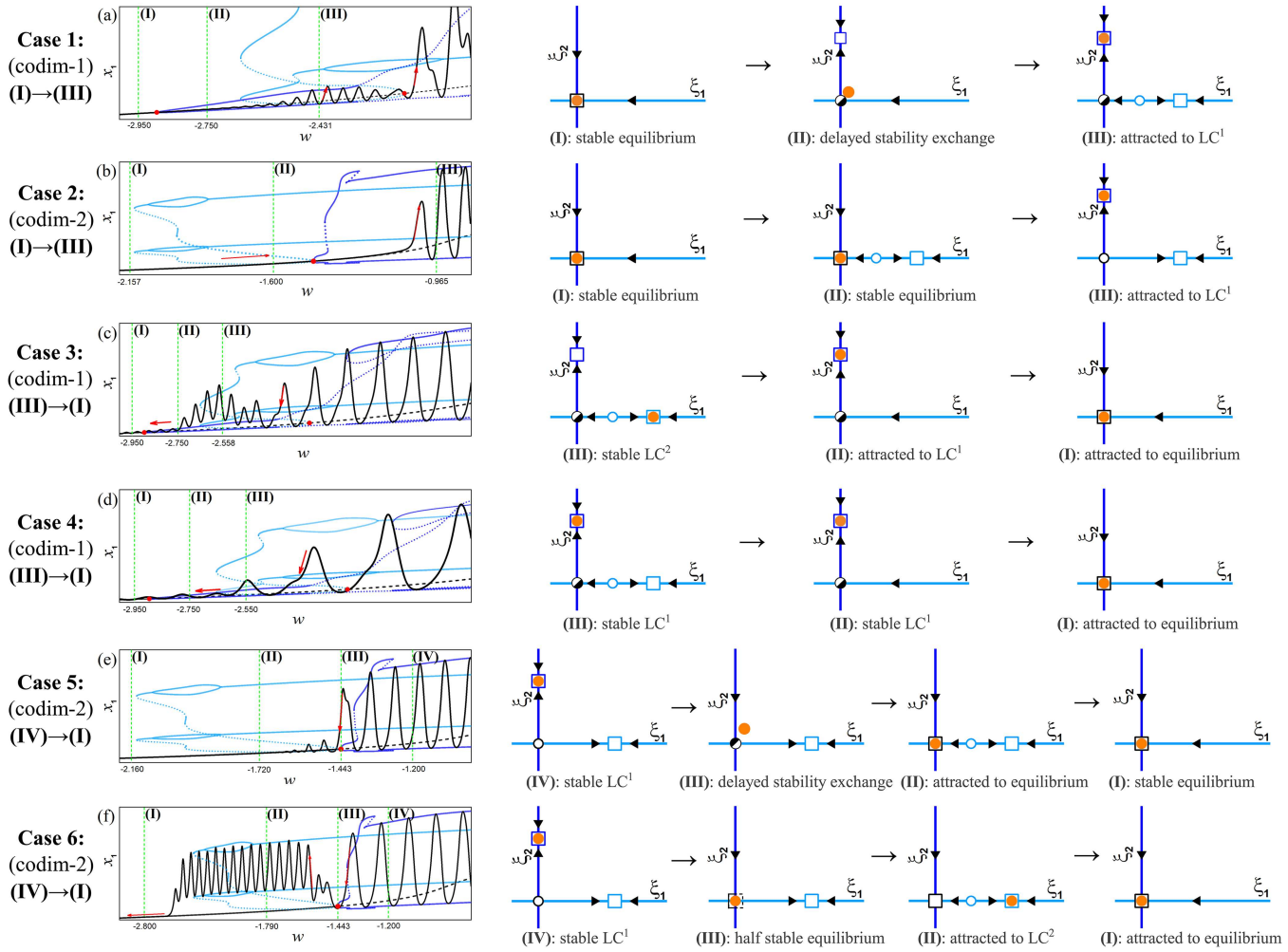

FIG. 7. The fast subsystem phase portraits. The dots represent the bursting trajectory (orange), equilibrium points(black), and limit cycles (dark blue and light blue). The colored boxes represent stable attractors. (a) Codimension-1 case with increasing $w(t)$; (b) codimension-2 case with increasing $w(t)$; (c) codimension-1 two-mode case with decreasing $w(t)$; (d) codimension-1 single-mode case with decreasing $w(t)$; (e) codimension-2 two-mode case with decreasing $w(t)$; (f) codimension-2 two-mode case with decreasing $w(t)$.

$M_w^{(i)} = U_w^{(i)} \Sigma_w^{(i)} (V_w^{(i)})^*$, where $U_w^{(i)}$ is a 5×5 unitary matrix and $\Sigma_w^{(i)}$ the diagonal matrix containing the singular values in the descending order. The vectors $v_{1,2,3}(w)$ are defined as the first three columns of $U_w^{(1)}$ and $v'_{1,2,3}(w)$ as the first three columns of $U_w^{(2)}$.

At this point, we assume that the triple $v_1(w), v_2(w), v_3(w)$ are linearly independent, as well as $v'_1(w), v'_2(w), v'_3(w)$ for all w, which was the case in our simulations.

We define the coordinates ξ_1 and ξ_2 as the distances to the corresponding subspaces as

$$\begin{aligned} \xi_1(x(t)) &= \left\| \tilde{x}(t) - x(t)|_{V^{(1)}} \right\|, \\ \xi_2(x(t)) &= \left\| \tilde{x}(t) - x(t)|_{V^{(2)}} \right\|, \end{aligned} \tag{6}$$

where

$$\begin{aligned} x(t)|_{V^{(1)}} &= \langle \tilde{x}(t), v_1 \rangle v_1 + \langle \tilde{x}(t), v_2 \rangle v_2 + \langle \tilde{x}(t), v_3 \rangle v_3, \\ x(t)|_{V^{(2)}} &= \langle \tilde{x}(t), v'_1 \rangle v'_1 + \langle \tilde{x}(t), v'_2 \rangle v'_2 + \langle \tilde{x}(t), v'_3 \rangle v'_3. \end{aligned} \tag{7}$$

The similar coordinates for the limit cycles are given

$$\begin{aligned} \xi_1(\phi_w^{(i)}) &= \left\| \phi_w^{(i)}(w) - \phi_w^{(i)}(w)\big|_{V^{(1)}} \right\|, \\ \xi_2(\phi_w^{(i)}) &= \left\| \phi_w^{(i)}(w) - \phi_w^{(i)}(w)\big|_{V^{(2)}} \right\|, \end{aligned} \tag{8}$$

with $\phi_w^{(i)}(w)\big|_{V^{(1)}}$ and $\phi_w^{(i)}(w)\big|_{V^{(2)}}$ defined in a similar way as in (7).

The geometric meaning of the coordinates ξ_1, ξ_2 are the distances to the subspaces containing the limit cycles $\phi_w^{(1)}(t)$ and $\phi_w^{(2)}(t)$ from the branches $\mathrm{LC}^{(1)}$ and $\mathrm{LC}^{(2)}$, respectively. The reason for choosing the 3D subspaces $V^{(1)}$ and $V^{(2)}$ (as opposed to 2D) is that

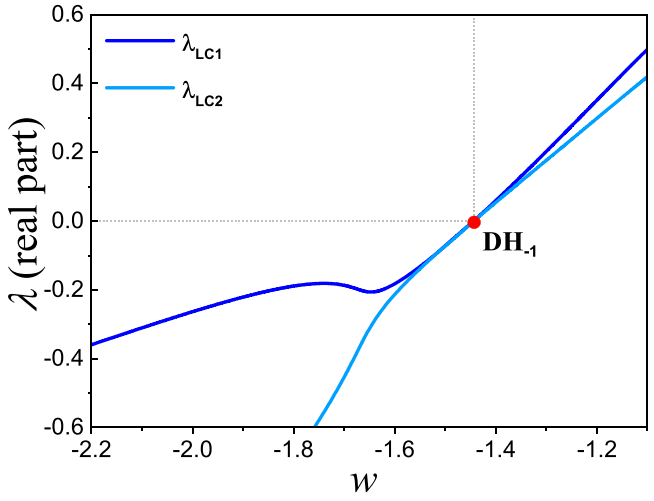

FIG. 8. The real part of two pairs of conjugate eigenvalues in the neighborhood of double-Hopf bifurcation DH_{-1}.

the 2D subspace spans the periodic solutions well only in the vicinity of the Hopf bifurcation. Far from the bifurcation, as in our example, the shapes of the limit cycles become more complex, which is more appropriate to embed in a 3D subspace.

Figure 6 shows one period of the bursting solution $\tilde{x}(t)$ as well as its the projection on $(\xi_1(t), \xi_2(t))$ plane for two bursting solutions. The blue curves as well as the light blue curves represent two different spiking modes, while the black lines represent the quiescent movements close to the equilibrium.

One can observe that the blue oscillations come close to the vertical axis $\xi_1 = 0$, while the light blue oscillations stick to the horizontal axis $\xi_2 = 0$, which corresponds to the movements close to subspaces $V^{(1)}$ and $V^{(2)}$, respectively. Furthermore, the single-mode bursting only exhibits oscillations close to the vertical axis, which is in agreement with the projection procedure. Similarly, we can project the limit cycles on the ξ_1, ξ_2 plane. For simplicity, here we use dots on the axes to show the positions of the limit cycles corresponding to w in Fig. 7. Note that the parameter w changes periodically from $-A$ to A for the bursting solution, and the positions of the limit cycles change along the corresponding axes, we only take the maximum value of $\xi_1(\phi_w^{(i)})$ and $\xi_2(\phi_w^{(i)})$, shown by the dots on the axes in Fig. 7.

Now, using the projections onto the plane (ξ_1, ξ_2), we will demonstrate that, for sufficiently small ε, the bursting episode always (for both codimension-1 and codimension-2 cases) starts with the $LC^{(1)}$ fast oscillations, when the absolute value of w decreases, or equivalently $|x_1|$ decreases, see Figs. 3(c) and 3(f), 4(c) and 4(f), and 5(a). This is described by Cases 1 and 2 below.

Case 1: codimension-1 case with increasing $w(t)$ from the minimal value is shown schematically in Fig. 7(a). For positive w, the scenario is symmetric. The phase point is firstly attracted by the stable equilibrium in (I) and then moves to the "dark blue" limit cycle $LC^{(1)}$ in (III) because it is the only stable attractor in the fast vector field. This transition is delayed with respect to the stability loss of the equilibrium as it is expected in the case of a slowly changing parameter,[41,42] see (II).

Case 2: codimension-2 case with increasing $w(t)$ from the minimal value is shown schematically in Fig. 7(b). When w moves from (I) to (III), the phase state stays at the equilibrium branch in (I) and can be attracted by two coexisting limit cycles in (III), since these are two stable attractors remaining after the equilibrium loses its stability. However, the trajectory approaches the "dark blue" limit cycle $LC^{(1)}$. The reason for such a behavior can be explained by the dependence of the real parts of the eigenvalues of the equilibrium shown in Fig. 8. There, the eigenvalues corresponding to the destabilization of the "dark blue" limit cycle are shown in the dark blue color and otherwise in the light blue. We observe that the real parts of the eigenvalues from Fig. 8 corresponding to both limit cycles are tangent, but the second derivative for the eigenvalues in the direction of the "dark blue" limit cycle is larger. As a result, the standard theory for delayed exchange of stability can be applied, leading to the orbit jumping in the direction of the "dark blue" limit cycle. We do not go into further detail here and refer to, e.g., Refs. 41–46.

The next cases correspond to the tails of the bursting episodes, i.e., when $|w|$ decreases. In the both codimension-1 and codimension-2 cases, the single- and two-mode can be realized.

Case 3: codimension-1 two-mode case with decreasing $w(t)$ in $w \in (-2.0, -3.0)$ is shown schematically in Fig. 7(c). When w decreases from (III) to (I), the phase point is first attracted by $LC^{(2)}$ in (III), behaving in one spiking state SP_3 to SP_4 in Fig. 3(b). When w decreases to (II), due to the disappearance of $LC^{(2)}$, the phase point turns to monostable $LC^{(1)}$ and finally settles down to the stable equilibrium in (I), resulting in the quiescent state.

Case 4: codimension-1 single-mode case with decreasing $w(t)$ in $w \in (-2.0, -3.0)$ is presented in Fig. 7(d). Unlike the scenario in Case 3, the phase point is attracted to $LC^{(1)}$ in (III), leading to small-amplitude oscillations. When it goes to (II) since no other bifurcation $LC^{(1)}$ of takes place, the phase point remains on $LC^{(1)}$ and settles down to the equilibrium in the case (I). Apparently, a stronger slow passage effect delays the ending of oscillations according to $LC^{(1)}$, causing phase point to be attracted to $LC^{(1)}$ in (III), which leads to the disappearance of a burst of the $LC^{(2)}$ spiking state compared to case 3. We do not prove the latter conjecture in more rigor as it is outside of the scope of this paper.

The slow passage effect in such slowly excited system is determined by the excitation frequency and the excitation amplitude, i.e., single-mode for larger A and ε while two-mode for smaller A and ε, which is consistent with the distributions shown in Fig. 5(b). However, it works differently in Fig. 5(c), implying different transition patterns at the codimension-2 bifurcation point. To explain the details, we also describe the fast subsystem phase portraits at the codimension-2 double-Hopf bifurcation point in the following cases 5 and 6.

Case 5: codimension-2 single-mode case with decreasing $w(t)$ in $w \in (-1.0, -2.2)$ is in Fig. 7(e). Similar to codimension-1 cases, the phase point stays on the stable limit cycle $LC^{(1)}$ in (IV). When w goes from (IV) to (III), due to the delay effect, the phase point continues to oscillate according to $LC^{(1)}$ at the double-Hopf bifurcation point and gradually settles down on a stable equilibrium, shown in (II).

Case 6: codimension-2 two-mode case with decreasing $w(t)$ in $w \in (-1.0, -3.0)$ is presented in Fig. 7(f). The phase point in (IV)

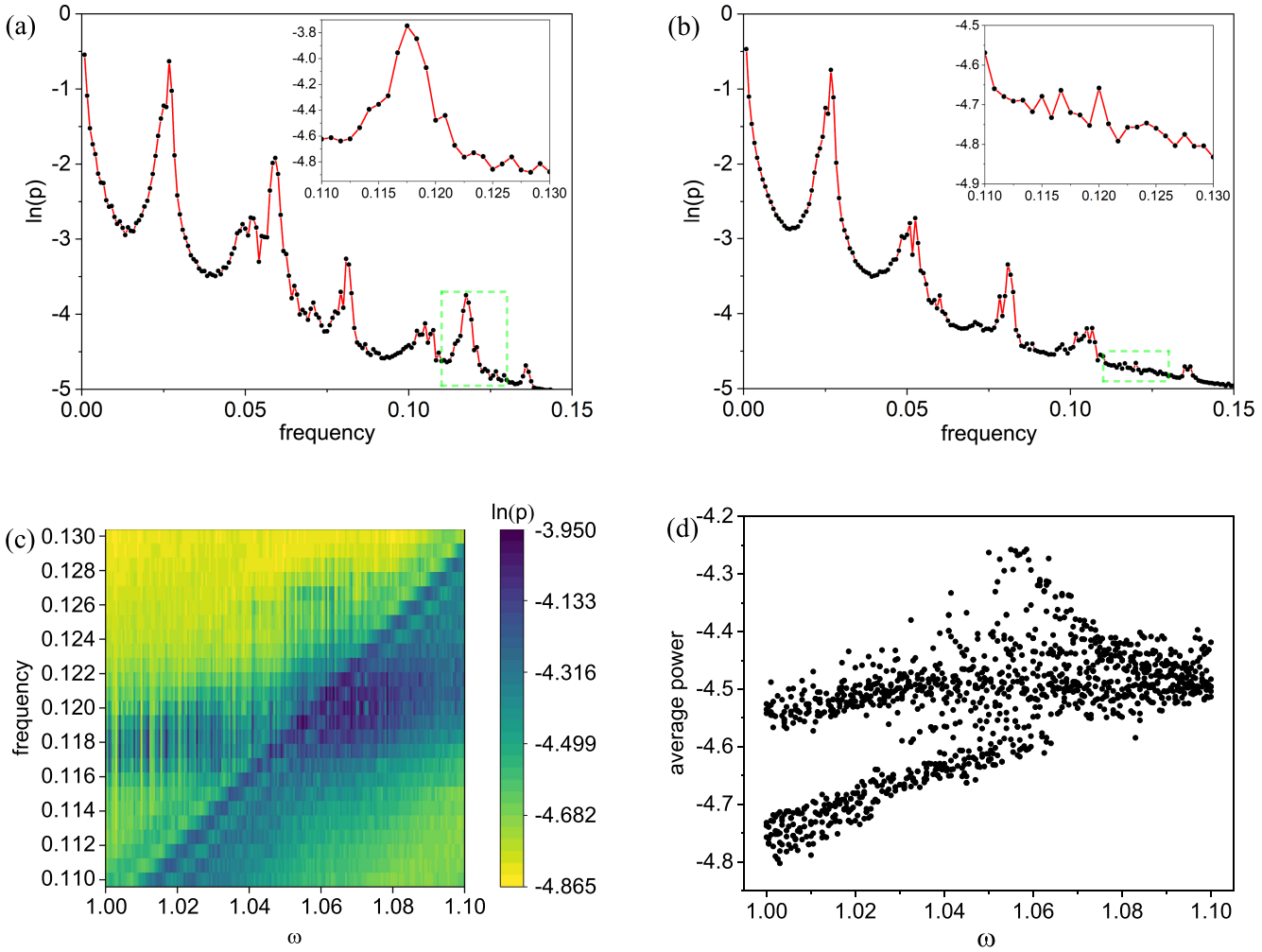

FIG. 9. The distribution of bursting multistability. (a) and (b) the power spectra of the two-mode bursting and the single-mode bursting in codimension-2 case for $A = 3.90$ and $A = 4.90$, excitation frequency fixed at $\varepsilon = 0.002$; (c) the heatmap with variation of ω in frequency band $(0.11, 0.13)$; (d) the average power with variation of ω in frequency band $(0.11, 0.13)$.

goes from $LC^{(1)}$ to a semi-stable equilibrium in (III) at the bifurcation point. Since only the stable attractor $LC^{(2)}$ exists in the vector field, it then jumps to $LC^{(2)}$ in (II), corresponding to the transitions between the two spiking states SP_3 and SP_4 in Fig. 4(b). When w decreases to phase (I), the point settles down to the equilibrium.

In codimension-2 cases, the delay effects still exist, resulting in different positions of the phase point at the double-Hopf bifurcation, which further determines which attractor to turn to. Specifically, A and ε can affect the number of oscillations according to $LC^{(1)}$, see segments for $w \in (-1.443, -1.200)$ in Figs. 7(e) and 7(f), which further changes the position of phase point when w reaches the bifurcation point. As a result, there is always a chance that the phase point visits the semi-stable equilibrium in (III), causing the two-mode bursting. Note that a relatively small excitation amplitude, or a relatively small excitation frequency, would increase the frequency of spiking oscillations, corresponding to a larger probability of the phase point to be attracted to the semi-stable point, which matches a denser distribution on the left side of Fig. 5(c). We refer to such a property as the *mixing double-Hopf effect*, i.e., the double-Hopf bifurcation leads to the coexistence of both single- and two-mode bursting for small ε, as it is observed in the left side of Fig. 5(c).

VI. ROBUSTNESS OF THE DOUBLE-HOPF MIXING EFFECT

In Secs. III–V, we only consider two-parameter sets, namely, $\omega = 1.1$ for codimension-1 Hopf bifurcations and $\omega = 1.0$ for codimension-2 double-Hopf bifurcations. Here, we investigate the

robustness of the observed mixing effect when the parameter value deviates from the exact value $\omega = 1.0$ of codimension-2 bifurcation.

To distinguish two-mode bursting from single-mode bursting, we employ the power spectra analysis to the bursting timeseries (Fig. 9). From the power spectra, we find that the two-mode bursting has an additional peak in the frequency band $(0.11, 0.13)$, corresponding to oscillations according to $LC^{(2)}$. Therefore, we obtain the distribution of two bursting solutions by computing the frequency spectra for different values of ω in Fig. 9(c). Here, we fix the excitation frequency at $\varepsilon = 0.002$ and pick one random excitation amplitude A from $(3.8, 6.0)$ for each ω.

The dark blue stripes in the frequency range $(0.116, 0122)$ in Fig. 9 represent the two-mode bursting, while the yellow stripes represent the single-mode bursting. The left part of the figure Fig. 9 shows the interchanging stripes of both kinds, which indicate the bursting multistability in the range of ω from $\omega = 1.0$ to $\omega \approx 1.06$. In addition, when $\omega \gtrsim 1.06$, all stripes are in dark blue, implying only two-mode bursting.

To further verify the robustness of the double-Hopf effect, we also compute the average power for each bifurcation parameter w in the frequency band $(0.11, 0.13)$ [Fig. 9(d)]. Therefore, we clearly see the two groups of average power from $\omega = 1.0$ to $\omega \approx 1.06$.

Thus, we have shown that the double-Hopf mixing effect takes place not only at the parameter values exactly at the double-Hopf bifurcation, but also in a small neighborhood of it, i.e., the effect is robust under a variation of parameters.

VII. CONCLUSION AND DISCUSSION

The present paper has been aimed at highlighting the distinction between bursting emerging due to codimension-1 or codimension-2 bifurcations of the fast subsystem. In this paper, we have studied the bursting oscillations in a coupled BVP oscillator with a slow-varying periodic excitation. We have presented two solutions of bursting oscillations with double-Hopf bifurcation, i.e., the single-mode bursting and the two-mode bursting. As a comparison, we have also performed a perturbation to the parameter set to obtain the two bursting solutions with codimension-1 Hopf bifurcation. Specifically, codimension-1 Hopf bifurcation and codimension-2 double-Hopf bifurcation can both cause multistability and further result in two bursting solutions, while codimension-2 double-Hopf bifurcation can lead to stable coexistence of two bursting solutions, namely, bursting multistability, which we called the *double-Hopf mixing effect*. We find that the delay effect works differently in two cases. That is, when we increase the excitation frequency, the stronger delay effect appears, resulting in the single distribution of single-mode bursting in the codimension-1 case. However, for the codimension-2 case, although the delay effect leads to the reduction of two-mode bursting, the coexistence of two bursting solutions still exists. To understand the transition mechanism between different stable attractors as well as the mechanism of bursting multistability, we have employed the fast subsystem phase portraits. Furthermore, we have explored the robustness of the double-Hopf effect on bursting multistability.

This work sheds some light on complex slow–fast dynamics in slow–fast systems with codimension-2 bifurcations. Other codimension-2 bifurcations, such as the fold–Hopf and the pitchfork–Hopf bifurcations, may require further investigation due to the different multistabilities they possess. Another possible extension is that our result can be helpful to explore rate-induced tipping with codimension-2 bifurcations. We also hope to extend this study to climate systems so that it may help to better understand the multiroute tipping scenarios close to double-Hopf bifurcation.

The observed bursting solutions contain several very challenging tipping scenarios and delayed exchange effects as ingredients, so it would be worthwhile to study some of the scenarios in more detail in the future.

ACKNOWLEDGMENTS

The authors would like to thank the financial support from Chinese Scholarship Council (CSC) under Grant No. 202108320327 (Y.X.); German Research Foundation DFG, Project No. 411803875 (S.Y.); and National Natural Science Foundations of China under Grant Nos. 11632008 and 11972173 (Q.B.).

AUTHOR DECLARATIONS

Conflict of Interest

The authors have no conflicts to disclose.

Author Contributions

Yibo Xia: Formal analysis (lead); Visualization (lead); Writing – original draft (equal). **Serhiy Yanchuk:** Methodology (lead); Writing – original draft (equal). **Yichuan Cao:** Software (lead). **Qinsheng Bi:** Conceptualization (lead); Funding acquisition (lead); Supervision (equal); Writing – review & editing (equal). **Jürgen Kurths:** Supervision (equal); Writing – review & editing (equal).

DATA AVAILABILITY

The data that support the findings of this study are available from the corresponding author upon reasonable request.

APPENDIX A: BIFURCATION ANALYSIS OF THE GENERALIZED AUTONOMOUS SYSTEM

For the excited system (3), we fix the excitation frequency at a relatively small value, which is far less than the natural frequency, implying two scales involved in the frequency domain. Due to this order gap between two frequencies, when the state variables oscillate according to the natural frequency, the excitation term w remains nearly constant. For example, in any period T_N related to the natural frequency ω_N, w changes from $w_{t_0} = A\sin(\varepsilon t_0)$ to $w_{t_N} = A\sin[\varepsilon(t_0 + T_N)]$, suggesting that $w_{t_0} \approx w_{t_N}$. Based on above analysis we can regard the whole excitation term w as a slow-varying parameter varying from $-A$ to A, and, thus, we can obtain the equilibrium branches as well as the bifurcations in fast subsystems.

The equilibrium points can be expressed in the form

$$x_E = (x_1, y_1, x_2, y_2, x_3) = \left(\frac{\omega Y_1}{\sigma}, Y_1, \frac{\omega Y_2}{\sigma}, Y_2, \frac{\omega_0 (Y_1 - Y_2)}{\sigma_0}\right), \tag{A1}$$

where the relation between Y_1 and Y_2 can be described as

$$\begin{cases} -\gamma\, {Y_1}^5 - \beta\, {Y_1}^3 - \alpha\, Y_1 - \dfrac{\omega^2 Y_1}{\sigma} - \dfrac{{\omega_0}^2 (Y_1 - Y_2)}{\sigma_0} + w = 0, \\ -\gamma\, {Y_2}^5 - \beta\, {Y_2}^3 - \alpha\, Y_2 - \dfrac{\omega^2 Y_2}{\sigma} + \dfrac{{\omega_0}^2 (Y_1 - Y_2)}{\sigma_0} = 0. \end{cases} \tag{A2}$$

Then, the stability of equilibrium points can be obtained by employing the characteristic equation, which can be expressed via introducing functions $f(\lambda)$ and $g(\lambda)$ for easy calculation, written in the form

$$F(\lambda) \equiv f(\lambda) g(\lambda) = \lambda^5 + c_1\lambda^4 + c_2\lambda^3 + c_3\lambda^2 + c_4\lambda + c_5 = 0, \tag{A3}$$

where

$$\begin{aligned} f(\lambda) &= \lambda^2 + a_1\lambda + a_2, \\ g(\lambda) &= \lambda^3 + b_1\lambda^2 + b_2\lambda + b_3, \\ c_1 &= a_1 + b_1 \\ &= S_1 + S_2 + 2\sigma + \sigma_0, \\ c_2 &= a_1 b_1 + a_2 + b_2 \\ &= \sigma^2 + (2S_1 + 2S_2 + 2\sigma_0)\sigma + (S_1 + S_2)\sigma_0 \\ &\quad + S_1 S_2 + 2\omega^2 + 2{\omega_0}^2, \\ c_3 &= a_1 b_2 + a_2 b_1 + b_3 \\ &= \left((2S_2 + 2\sigma_0) S_1 + 2S_2\sigma_0 + 2\omega^2 + 4{\omega_0}^2\right)\sigma \\ &\quad + (S_1 + S_2 + \sigma_0)\sigma^2 + \left(\omega^2 + {\omega_0}^2\right) S_2 + 2\omega^2\sigma_0 \\ &\quad + \left(S_2\sigma_0 + \omega^2 + {\omega_0}^2\right) S_1, \\ c_4 &= a_1 b_3 + a_2 b_2 \\ &= \left((S_1 + S_2 + 2\sigma_0)\omega^2 + 2S_1 S_2\sigma_0 + 2{\omega_0}^2 (S_1 + S_2)\right)\sigma \\ &\quad + \left((S_1 + S_2)\sigma_0 + S_1 S_2 + 2{\omega_0}^2\right)\sigma^2 \\ &\quad + \omega^2\left(\omega^2 + (S_1 + S_2)\sigma_0 + 2{\omega_0}^2\right), \\ c_5 &= a_2 b_3 \\ &= \left(S_1 S_2\sigma_0 + {\omega_0}^2 (S_1 + S_2)\right)\sigma^2 \\ &\quad + \left((S_1 + S_2)\sigma_0 + 2{\omega_0}^2\right)\omega^2\sigma + \omega^4\sigma_0, \end{aligned}$$

with $S_1 = 5\gamma\, {Y_1}^4 + 3\beta\, {Y_1}^2 + \alpha$ and $S_2 = 5\gamma\, {Y_2}^4 + 3\beta\, {Y_2}^2 + \alpha$.

According to the Routh–Hurwitz criterion, all solutions of (A3) would have negative real parts when the conditions are met,

$$\begin{cases} c_1 > 0, \\ c_5 > 0, \\ c_1 c_2 - c_3 > 0, \\ -{c_1}^2 c_4 + (c_2 c_3 + c_5)\, c_1 - {c_3}^2 > 0, \\ -{c_1}^2 {c_4}^2 - c_1 {c_2}^2 c_5 + c_1 c_2 c_3 c_4 \\ +2\, c_1 c_4 c_5 + c_2 c_3 c_5 - {c_3}^2 c_4 - {c_5}^2 > 0. \end{cases} \tag{A4}$$

With the variation of parameter w, the stability of equilibrium points E may change because of the appearance of different bifurcations in the vector field. When $F(\lambda)$ has a pair of purely imaginary roots, the Hopf bifurcation may take place, resulting in the transition from fixed point to a limit cycle. For the case when $f(\lambda)$ has conjugate imaginary roots while the roots of $g(\lambda)$ are all negative, the corresponding set can be expressed as

$$HB_1 : a_1 = 0, a_2 > 0, b_1 > 0, b_3 > 0, b_1 b_2 - b_3 > 0, \tag{A5}$$

and the associated oscillation frequency can be calculated at $\Omega_H = \sqrt{a_2}$. While when $g(\lambda)$ has a pair of purely imaginary roots and $f(\lambda)$ has all negative roots, the Hopf bifurcation appears on the set

$$HB_2 : a_1 > 0, a_1 a_2 - 1 > 0, b_2 > 0, b_1 b_2 - b_3 = 0, \tag{A6}$$

which may cause the oscillations with the frequency $\Omega_H = \sqrt{b_2}$. Furthermore, a codimension-2 bifurcation with two pairs of purely imaginary roots may take place, leading to two coexisting periodic oscillations in the phase space. The associated characteristic equation should have the form $F(\lambda) = (\lambda^2 + \varphi_1^2)(\lambda^2 + \varphi_2^2)(\lambda + \varphi_3) = 0$, where $\varphi_{1,2} \neq 0, \varphi_3 > 0$, implying that a double-Hopf bifurcation occurs on the set

$$DH : a_1 = 0, a_2 > 0, b_1 > 0, b_2 > 0, b_1 b_2 - b_3 = 0. \tag{A7}$$

Therefore, the characteristic equation $F(\lambda)$ can be simplified in the form

$$F(\lambda) = (\lambda^2 + a_2)(\lambda^2 + b_2)(\lambda + b_1), \tag{A8}$$

with two pairs of purely imaginary roots $\pm i\sqrt{a_2}$ and $\pm i\sqrt{b_2}$ as well as a negative root $-b_1$.

APPENDIX B: DYNAMICAL BEHAVIORS WITH CODIMENSION-1 HOPF BIFURCATIONS

When $\omega = 1.1$, the slow-varying parameter w crosses all the regions back and forth on the parameter plane, resulting in the occurrence of four Hopf bifurcations, see Fig. 2(a). Details of equilibrium branches, limit cycles, and the corresponding bifurcations are plotted in Fig. 10.

Since the equilibrium branches as well as those bifurcations keep symmetry on w, we only present the dynamics for $w < 0$. When $w < -2.8937$, only stable equilibrium point on EB_{-2} exists, shown in Fig. 10(e). With the increase of w, super-critical Hopf bifurcation at HB_{-2} for $w = -2.8937$ takes place, resulting in unstable equilibrium point EB_{-1} as well as stable limit cycle $\mathrm{LC}_{-2}^{(1)}$, see Fig. 10(c). For $w = -2.6549$, fold bifurcation of limit cycle LC^2 occurs, leading to stable limit cycle $\mathrm{LC}_{-2}^{(2)}$ that coexists with $\mathrm{LC}_{-2}^{(1)}$. For further variation of w, $\mathrm{LC}^{(2)}$ continues to evolve via twofold bifurcations of limit cycle for $w = -2.5062$ and $w = -2.4884$, which cause the appearance of stable $\mathrm{LC}_0^{(2)}$ as well as the disappearance of stable $\mathrm{LC}_{-2}^{(2)}$, respectively. Meanwhile, the unstable $\mathrm{LC}_{-3}^{(2)}$ disappears via sub-critical Hopf bifurcation at HB_{-2} when $w = -2.1892$, which also results in the unstable equilibrium branches EB_0.

When w increases to $w = -2.4172$, the period of $\mathrm{LC}_0^{(2)}$ is doubled due to period-doubling bifurcation and the sequence of period-doubling bifurcation occurs until $w = -2.0828$. Another type of bifurcation of limit cycle, namely, Neimark–Sacker bifurcation, takes place for $w = -2.3213$, yielding that the stable $\mathrm{LC}_{-2}^{(1)}$ loses the stability. Further stability changes of $\mathrm{LC}^{(1)}$ involves several

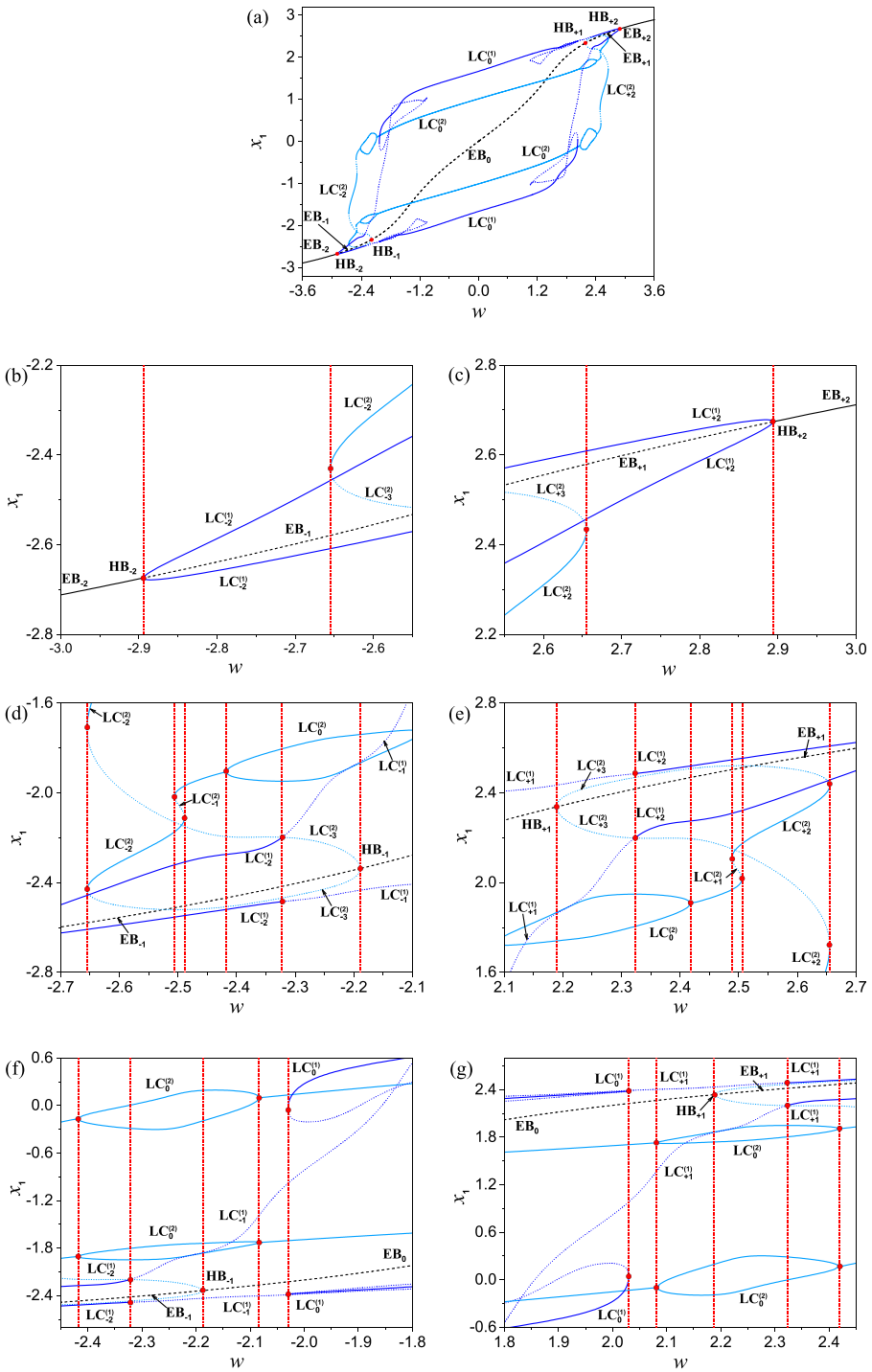

FIG. 10. Details of bifurcation diagram and the locally enlarged parts for codimension-1 case in Fig. 2(b).

fold bifurcations of limit cycle and it may finally become stable at $w = -2.0305$, shown in Fig. 10(a).

Here, we summarize the complex dynamical behaviors with variation of parameter w in Table I, from which one may find that different stable attractors coexist in many intervals of w, implying that there may be different forms of oscillations coexisting with different initial values are taken in each interval.

TABLE I. Evolution of the dynamics with the variation of w in the codimension-1 case.

Variation of w	The dynamical behavior
$w < -2.8937$	Stable equilibrium branch EB_{-2}
$w = -2.8937$	Super-critical Hopf bifurcation HB_{-2}
$w \in (-2.8937, -2.6549)$	Stable limit cycle $LC^{(1)}_{-2}$ and unstable EB_{-1}
$w = -2.6549$	Fold bifurcation of limit cycle $LC^{(2)}$ connecting $LC^{(2)}_{-2}$ and $LC^{(2)}_{-3}$
$w \in (-2.6549, -2.5062)$	Stable $LC^{(1)}_{-2}$ and $LC^{(2)}_{-2}$ unstable $LC^{(2)}_{-3}$ and unstable EB_{-1}
$w = -2.5062$	Fold bifurcation of limit cycle $LC^{(2)}$ connecting $LC^{(2)}_{0}$ and $LC^{(2)}_{-1}$
$w \in (-2.5062, -2.4884)$	Stable $LC^{(1)}_{-2}$, $LC^{(2)}_{-2}$ and $LC^{(2)}_{0}$ unstable $LC^{(2)}_{-3}$ and $LC^{(2)}_{-1}$ unstable EB_{-1}
$w = -2.4884$	Fold bifurcation of limit cycle $LC^{(2)}$ connecting $LC^{(2)}_{-1}$ and $LC^{(2)}_{-2}$
$w \in (-2.4884, -2.4172)$	Stable $LC^{(1)}_{-2}$ and $LC^{(2)}_{0}$ unstable $LC^{(2)}_{-3}$ and unstable EB_{-1}
$w = -2.4172$	Period-doubling bifurcation of $LC^{(2)}$
$w \in (-2.4884, -2.4172)$	Period-2 of $LC^{(2)}_{0}$ and stable $LC^{(1)}_{-2}$ unstable $LC^{(2)}_{-3}$ and unstable EB_{-1}
$w = -2.3213$	Neimark–Sacker bifurcation of $LC^{(1)}$ connecting $LC^{(1)}_{-2}$ and $LC^{(1)}_{-1}$
$w \in (-2.3213, -2.1892)$	Period-2 of $LC^{(2)}_{0}$ unstable $LC^{(2)}_{-3}$ and $LC^{(1)}_{-1}$ unstable EB_{-1}
$w = -2.1892$	Sub-critical Hopf bifurcation HB_{-1}
$w \in (-2.1892, -2.0828)$	Period-2 of $LC^{(2)}_{0}$ unstable $LC^{(1)}_{-1}$ and unstable EB_{0}
$w = -2.0828$	Reverse period-doubling bifurcation of $LC^{(2)}$
$w \in (-2.0828, -2.0305)$	Stable $LC^{(2)}_{0}$ unstable $LC^{(1)}_{-1}$ and unstable EB_{0}
$w = -2.0305$	Fold bifurcation of limit cycle $LC^{(1)}$ connecting $LC^{(1)}_{-1}$ and $LC^{(1)}_{0}$
$w \in (-2.0305, 0]$	Stable $LC^{(1)}_{0}$, $LC^{(2)}_{0}$ and unstable EB_{0}

APPENDIX C: DYNAMICAL BEHAVIORS WITH DOUBLE-HOPF BIFURCATIONS

So far, we have obtained the complex dynamics with codimension-1 Hopf bifurcations when parameter w crosses all regions for $\omega = 1.1$ in Appendix B. While when $\omega = 1.0$, the slow-varying parameter travels across three regions, which may lead to different dynamics since double-Hopf bifurcations take place. we also summarize the complex dynamics with double-Hopf bifurcations in Table II and plot the details in Fig. 11.

Here, we only present the dynamics for $w < 0$ because of the symmetry. When $w < -2.1412$, only stable equilibrium points on EB_{-1} exists, shown in Fig. 11(b). With the increase of w, the unstable $LC^{(2)}_{-1}$ and the stable $LC^{(2)}_{-1}$ meet at $w = -2.1412$, yielding the occurrence of the fold bifurcation of limit cycle $LC^{(2)}$. When $w = -2.0858$, the period-doubling bifurcation of $LC^{(2)}$ takes place, resulting in period-2 limit cycle $LC^{(2)}_{0}$. The unstable $LC^{(2)}_{-1}$, with further increase of w, changes the stability via another fold bifurcation of $LC^{(2)}$ at -1.9727, causing stable $LC^{(2)}_{-2}$ to coexist with period-2 $LC^{(2)}_{0}$. Another fold bifurcation of $LC^{(2)}$ occurring at -1.9763 may further change the stability of $LC^{(2)}_{-2}$, leading to unstable $LC^{(2)}_{-3}$. Further changes of $LC^{(2)}$ takes place because of the reverse period-doubling bifurcation at $w = -1.8564$, which restores the $LC^{(2)}_{0}$ to period-1 type.

When w increases to $w = -1.4441$, double-Hopf bifurcation DH_{-1} occurs, resulting in the appearance of unstable equilibrium points EB_0 as well as stable $LC^{(1)}_{-4}$, together with the disappearance

TABLE II. Evolution of the dynamics with the variation of w in the codimension-2 case.

Variation of w	The dynamical behavior
$w < -2.1412$	Stable equilibrium branch EB_{-1}
$w = -2.1412$	Fold bifurcation of limit cycle $LC^{(2)}$ connecting $LC^{(2)}_{-1}$ and $LC^{(2)}_{0}$
$w \in (-2.1412, -2.0858)$	Stable limit cycle $LC^{(2)}_{0}$ unstable $LC^{(2)}_{-1}$ and stable EB_{-1}
$w = -2.0858$	Period-doubling bifurcation of $LC^{(2)}$
$w \in (-2.0858, -1.9763)$	Period-2 of $LC^{(2)}_{0}$ unstable $LC^{(2)}_{-1}$ and stable EB_{-1}
$w = -1.9763$	Fold bifurcation of limit cycle $LC^{(2)}$ connecting $LC^{(2)}_{-3}$ and $LC^{(2)}_{-2}$
$w \in (-1.9763, -1.9727)$	Period-2 of $LC^{(2)}_{0}$, stable $LC^{(2)}_{-2}$ unstable $LC^{(2)}_{-1}$, $LC^{(2)}_{-3}$ and stable EB_{-1}
$w = -1.9727$	Fold bifurcation of limit cycle $LC^{(2)}$ connecting $LC^{(2)}_{-2}$ and $LC^{(2)}_{-1}$
$w \in (-1.9727, -1.8564)$	Period-2 of $LC^{(2)}_{0}$ unstable $LC^{(2)}_{-3}$ and stable EB_{-1}
$w = -1.8564$	Reverse period-doubling bifurcation of $LC^{(2)}_{0}$
$w \in (-1.8564, -1.4441)$	Stable $LC^{(2)}_{0}$ unstable $LC^{(2)}_{-3}$ and unstable EB_{-1}
$w = -1.4441$	Double-Hopf bifurcation DH_{-1}
$w \in (-1.4441, -1.3998)$	Stable $LC^{(2)}_{0}$, $LC^{(1)}_{-4}$ unstable EB_{-1}
$w = -1.3998$	Fold bifurcation of limit cycle $LC^{(1)}$ connecting $LC^{(1)}_{-3}$ and $LC^{(1)}_{-2}$
$w \in (-1.3998, -1.3882)$	Stable $LC^{(1)}_{-4}$, $LC^{(1)}_{-2}$, $LC^{(2)}_{0}$ unstable $LC^{(1)}_{-3}$ and unstable EB_{0}
$w = -1.3882$	Fold bifurcation of limit cycle $LC^{(1)}$ connecting $LC^{(1)}_{-4}$ and $LC^{(1)}_{-3}$
$w \in (-1.3882, -1.3167)$	Stable $LC^{(1)}_{-2}$, $LC^{(2)}_{0}$ unstable EB_{0}
$w = -1.3167$	Fold bifurcation of limit cycle $LC^{(1)}$ connecting $LC^{(1)}_{-1}$ and $LC^{(1)}_{0}$
$w \in (-1.3167, -1.2657)$	Stable $LC^{(1)}_{-2}$, $LC^{(1)}_{0}$, $LC^{(2)}_{0}$ unstable $LC^{(1)}_{-1}$ and unstable EB_{0}
$w = -1.2657$	Fold bifurcation of limit cycle $LC^{(1)}$ connecting $LC^{(1)}_{-2}$ and $LC^{(1)}_{-1}$
$w \in (-1.2657, 0]$	Stable $LC^{(1)}_{0}$, $LC^{(2)}_{0}$ unstable EB_{0}

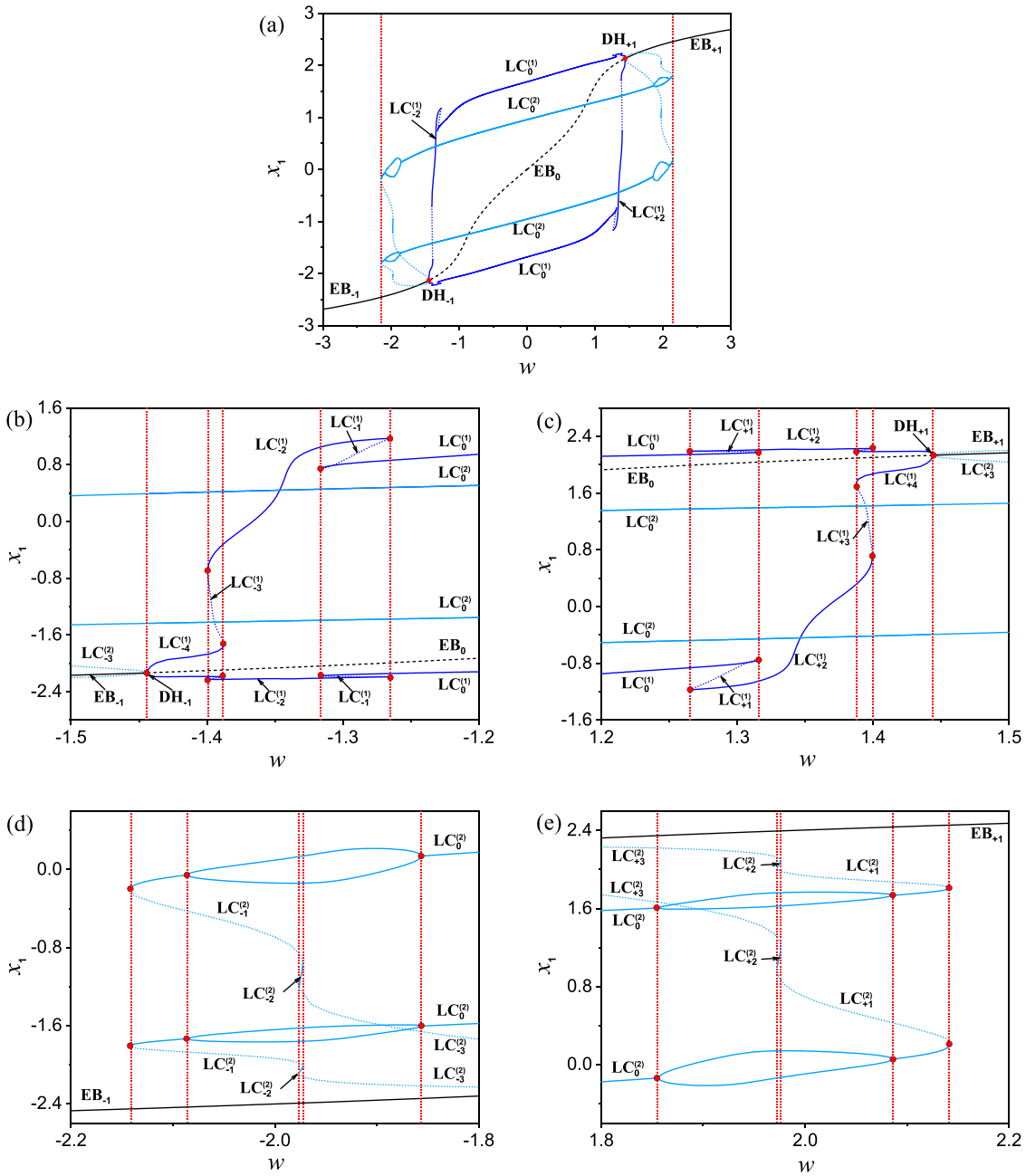

FIG. 11. Details of bifurcation diagram and the locally enlarged parts for the codimension-2 case in Fig. 2(c).

of unstable $LC^{(2)}_{-3}$, shown in Fig. 11(d). Further variation of w causes the $LC^{(1)}_{-4}$ to evolve via the folds of limit cycle, more specifically, the folds of $LC^{(1)}$ at $w = -1.3998$ and $w = -1.3882$ changes the stability, leading to stable $LC^{(1)}_{-2}$ and unstable $LC^{(1)}_{-3}$. Similarly, the folds of $LC^{(1)}$ at $w = -1.3167$ and $w = -1.2657$ connect two stable limit cycles $LC^{(1)}_{-2}$ as well as $LC^{(1)}_{0}$ with unstable $LC^{(1)}_{-1}$. Therefore, when $w > -1.4441$, there coexist stable limit cycles $LC^{(2)}_{0}$ and $LC^{(1)}_{-4}$, which may lead to different forms of oscillations.

APPENDIX D: TERMINOLOGY

Here, we list important terminology in Table III.

TABLE III. Terminology involved.

Name	Description
Bursting oscillations	Oscillations that alternates with large-amplitude and small-amplitude oscillations or at rest
Spiking state	Large-amplitude oscillations in bursting oscillations
Quiescent state	Small-amplitude oscillations or at rest in bursting oscillations
Bursting multistability	Two bursting solutions coexist with different excitation amplitude and excitation frequency
Single-mode bursting	Bursting oscillations with single spiking state
Two-mode bursting	Bursting oscillations with the appearance of two spiking states
Double-Hopf mixing effect	Double-Hopf bifurcation leads to the appearance of bursting multistability for the range of considered excitation frequency.

REFERENCES

[1]A. L. Hodgkin and A. F. Huxley, "A quantitative description of membrane current and its application to conduction and excitation in nerve," J. Physiol. **117**, 500 (1952).
[2]A. Mielke, *Analysis, Modeling and Simulation of Multiscale Problems*, edited by A. Mielke (Springer, Berlin, 2006), pp. 1–697.
[3]T. Malashchenko, A. Shilnikov, and G. Cymbalyuk, "Six types of multistability in a neuronal model based on slow calcium current," PLoS One **6**, e21782 (2011).
[4]C. Kuehn, *Springer* (Springer-Verlag GmbH, 2015), Vol. 191, pp. 814.
[5]J. Cabral, M. L. Kringelbach, and G. Deco, "Functional connectivity dynamically evolves on multiple time-scales over a static structural connectome: Models and mechanisms," NeuroImage **160**, 84–96 (2017).
[6]M. Wechselberger, *Geometric Singular Perturbation Theory Beyond the Standard Form*, Frontiers in applied dynamical systems: Reviews and tutorials (Springer, Cham, 2020), Vol. 6.
[7]C. Siettos and J. Starke, "Multiscale modeling of brain dynamics: From single neurons and networks to mathematical tools," Wiley Interdiscip. Rev.: Syst. Biol. Med. **8**, 438–458 (2016).
[8]V. Petrov, S. K. Scott, and K. Showalter, "Mixed-mode oscillations in chemical systems," J. Chem. Phys. **97**, 6191–6198 (1992).
[9]D. Bakeš, L. Schreiberová, I. Schreiber, and M. J. Hauser, "Mixed-mode oscillations in a homogeneous pH-oscillatory chemical reaction system," Chaos **18**, 015102 (2008).
[10]J. Guckenheimer and C. Scheper, "A geometric model for mixed-mode oscillations in a chemical system," SIAM J. Appl. Dyn. Syst. **10**, 92–128 (2011).
[11]M. Desroches, J. Guckenheimer, B. Krauskopf, C. Kuehn, H. M. Osinga, and M. Wechselberger, "Mixed-mode oscillations with multiple time scales," SIAM Rev. **54**, 211–288 (2012).
[12]M. Krupa, N. Popović, N. Kopell, and H. G. Rotstein, "Mixed-mode oscillations in a three time-scale model for the dopaminergic neuron," Chaos **18**, 015106 (2008).
[13]G. De Vries and A. Sherman, "Channel sharing in pancreatic β-cells revisited: Enhancement of emergent bursting by noise," J. Theor. Biol. **207**, 513–530 (2000).
[14]S. Yanchuk and M. Wolfrum, "A multiple time scale approach to the stability of external cavity modes in the Lang–Kobayashi system using the limit of large delay," SIAM J. Appl. Dyn. Syst. **9**, 519–535 (2010).
[15]I. Bačić, S. Yanchuk, M. Wolfrum, and I. Franović, "Noise-induced switching in two adaptively coupled excitable systems," Eur. Phys. J. Spec. Top. **227**, 1077–1090 (2018).
[16]I. Franović, S. Yanchuk, S. Eydam, I. Bačić, and M. Wolfrum, "Dynamics of a stochastic excitable system with slowly adapting feedback," Chaos **30**, 083109 (2020).
[17]E. Mosekilde, B. Lading, S. Yanchuk, and Y. Maistrenko, "Bifurcation structure of a model of bursting pancreatic cells," BioSystems **63**, 3–13 (2001).
[18]J. Rinzel, "Bursting oscillations in an excitable membrane model," in *Ordinary and Partial Differential Equations: Proceedings of the Eighth Conference held at Dundee, Scotland, June 25–29, 1984* (Springer, 2006), pp. 304–316.
[19]R. Bertram, M. J. Butte, T. Kiemel, and A. Sherman, "Topological and phenomenological classification of bursting oscillations," Bull. Math. Biol. **57**, 413–439 (1995).
[20]C. Kuehn, "A mathematical framework for critical transitions: Bifurcations, fastslow systems and stochastic dynamics," Phys. D: Nonlinear Phenom. **240**, 1020–1035 (2011).
[21]E. M. Izhikevich, "Neural excitability, spiking and bursting," Int. J. Bifurcat. Chaos **10**, 1171–1266 (2000).
[22]J. Llibre, M. Messias, and A. de Carvalho Reinol, "Zero–Hopf bifurcations in three-dimensional chaotic systems with one stable equilibrium," Int. J. Bifurcat. Chaos **30**, 2050189 (2020).
[23]J. Li, Y. Liu, and Z. Wei, "Zero-Hopf bifurcation and Hopf bifurcation for smooth Chua's system," Adv. Differ. Equ. **2018**, 1–17 (2018).
[24]X. Li and Q. Bi, "Cusp bursting and slow-fast analysis with two slow parameters in photosensitive Belousov—Zhabotinsky reaction," Chin. Phys. Lett. **30**, 070503 (2013).
[25]Q. Bi, S. Li, J. Kurths, and Z. Zhang, "The mechanism of bursting oscillations with different codimensional bifurcations and nonlinear structures," Nonlinear Dyn. **85**, 993–1005 (2016).
[26]L. Duan and Q. Lu, "Bursting oscillations near codimension-two bifurcations in the Chay neuron model," Int. J. Nonlinear Sci. Numer. Simul. **7**, 59–64 (2006).
[27]F. Takens, H. W. Broer, B. Krauskopf, and G. Vegter, "Global analysis of dynamical systems: Festschrift dedicated to Floris Takens for his 60th birthday," Tech. Rep. (Institute of Physics Pub., 2001).
[28]L. Duan, Q. Lu, and Q. Wang, "Two-parameter bifurcation analysis of firing activities in the Chay neuronal model," Neurocomputing **72**, 341–351 (2008).
[29]W. H. Barnett and G. S. Cymbalyuk, "A codimension-2 bifurcation controlling endogenous bursting activity and pulse-triggered responses of a neuron model," PLoS One **9**, e85451 (2014).
[30]Y. Yu, Z. Zhang, and X. Han, "Periodic or chaotic bursting dynamics via delayed pitchfork bifurcation in a slow-varying controlled system," Commun. Nonlinear Sci. Numer. Simul. **56**, 380–391 (2018).
[31]Y. Xia, Z. Zhang, and Q. Bi, "Relaxation oscillations and the mechanism in a periodically excited vector field with Pitchfork–Hopf bifurcation," Nonlinear Dyn. **101**, 37–51 (2020).
[32]M. Golubitsky, K. Josic, and T. J. Kaper, "An unfolding theory approach to bursting in fast–slow systems," in *Global Analysis of Dynamical Systems* (CRC Press, 2001), pp. 282–313.
[33]Y. A. Kuznetsov, I. A. Kuznetsov, and Y. Kuznetsov, *Elements of Applied Bifurcation Theory* (Springer New York, 1998), Vol. 112.
[34]K. Tsumoto, T. Yoshinaga, and H. Kawakami, "Bifurcations in synaptically coupled BVP neurons," Int. J. Bifurcat. Chaos Appl. Sci. Eng. **11**, 1053–1064 (2001).
[35]X. P. Wu and L. Wang, "Codimension-2 bifurcations of coupled BVP oscillators with hard characteristics," Appl. Math. Comput. **219**, 5303–5320 (2013).
[36]T. Ueta, H. Miyazaki, T. Kousaka, and H. Kawakami, "Bifurcation and chaos in coupled BVP oscillators," Int. J. Bifurcat. Chaos **14**, 1305–1324 (2004).
[37]S. Tsuji, T. Ueta, and H. Kawakami, "Bifurcation analysis of current coupled BVP oscillators," Int. J. Bifurcat. Chaos **17**, 837–850 (2007).
[38]X. Zhang, B. Zhang, X. Han, and Q. Bi, "On occurrence of sudden increase of spiking amplitude via fold limit cycle bifurcation in a modified Van der Pol–Duffing system with slow-varying periodic excitation," Nonlinear Dyn. **108**, 2097–2114 (2022).
[39]S. Wieczorek, C. Xie, and P. Ashwin, "Rate-induced tipping: Thresholds, edge states and connecting orbits," arXiv:2111.15497 [math.DS] (2021).

[40] A. Dhooge, W. Govaerts, and Y. A. Kuznetsov, "Matcont: A MATLAB package for numerical bifurcation analysis of ODEs," ACM Trans. Math. Softw. **29**, 141–164 (2003).
[41] P. Ashwin, S. Wieczorek, R. Vitolo, and P. Cox, "Tipping points in open systems: Bifurcation, noise-induced and rate-dependent examples in the climate system," Philos. Trans. R. Soc. A: Math., Phys. Eng. Sci. **370**, 1166–1184 (2012). 1103.0169.
[42] S. M. Baer, T. Erneux, and J. Rinzel, "The slow passage through a Hopf bifurcation: Delay, memory effects, and resonance," SIAM J. Appl. Math. **49**, 55–71 (1989).
[43] C. Baesens, "Slow sweep through a period-doubling cascade: Delayed bifurcations and renormalisation," Phys. D **53**, 319–375 (1991).
[44] N. Berglund and H. Kunz, "Memory effects and scaling laws in slowly driven systems," J. Phys. A: Math. Gen. **32**, 15–39 (1999). 9807025.
[45] Y. Do and J. M. Lopez, "Slow passage through multiple bifurcation points," Discrete Contin. Dyn. Syst. B **18**, 95–107 (2013).
[46] J. Cantisán, S. Yanchuk, J. M. Seoane, M. A. F. Sanjuán, and J. Kurths, "Rate and memory effects in bifurcation-induced tipping," arXiv:2304.03668 (2023).